

Watershed Controls and Tropical Cyclone-Induced Changes in River Hydraulic Geometry in Puerto Rico

YIHAN LI¹, Daniel B Wright¹, and Brian P Bledsoe²

¹University of Wisconsin-Madison

²University of Georgia

November 22, 2022

Abstract

At-a-station hydraulic geometry (AHG), which describes how channel width, depth, and velocity vary with discharge at a river cross section, has long been used to study fluvial processes. For example, identification of landscape and river reach drivers of hydraulic geometry can help to predict channel properties at ungaged sites and to understand channel responses to major floods. Most prior AHG studies have focused on mid-latitude, temperate regions. Tropical zones—including those affected by tropical cyclones (TCs)—have received less attention. This study analyzed spatial and temporal variability in hydraulic geometry at 24 stream gaging sites in Puerto Rico, and identified the watershed and river reach characteristics that correlate with each hydraulic geometry parameter. These characteristics were then used to build regression models of AHG parameters, with relatively high predictive power. The largest flood events from each site were found to cause systematic changes to AHG parameters; most of these floods were caused by major TCs. Upstream drainage area, average watershed elevation, watershed land cover and other characteristics were found to be significant predictors of AHG parameters. Reaches with steeper slopes were found to have limited lateral adjustability, which may reflect consolidated bank materials and valley confinement. Watersheds with high percentages of forested area showed greater changes in roughness but less vertical adjustability than more developed watersheds. These correlation results help inform whether river channel properties in Puerto Rico and similar environments are resistant to the forces of TC-induced flooding, and how these properties are affected by major floods.

Hosted file

essoar.10508930.1.docx available at <https://authorea.com/users/534236/articles/598421-watershed-controls-and-tropical-cyclone-induced-changes-in-river-hydraulic-geometry-in-puerto-rico>

Hosted file

supplementary material.docx available at <https://authorea.com/users/534236/articles/598421-watershed-controls-and-tropical-cyclone-induced-changes-in-river-hydraulic-geometry-in-puerto-rico>

1 **Watershed Controls and Tropical Cyclone-Induced Changes in**
2 **River Hydraulic Geometry in Puerto Rico**

3 **Yihan Li^{a,*}, Daniel B. Wright^a, Brian P. Bledsoe^b**

4 **^a University of Wisconsin-Madison, 1415 Engineering Dr, Madison, Wisconsin 53706,**
5 **United States of America**

6 **^b University of Georgia, 200 D.W. Brooks Dr, Athens, Georgia 30602, United States of**
7 **America**

8 *** Corresponding Author. E-mail address: yihan.li@wisc.edu (Y. Li).**

9 **Abstract**

10 At-a-station hydraulic geometry (AHG), which describes how channel width, depth, and velocity
11 vary with discharge at a river cross section, has long been used to study fluvial processes. For
12 example, identification of landscape and river reach drivers of hydraulic geometry can help to
13 predict channel properties at ungaged sites and to understand channel responses to major floods.
14 Most prior AHG studies have focused on mid-latitude, temperate regions. Tropical zones—
15 including those affected by tropical cyclones (TCs)—have received less attention. This study
16 analyzed spatial and temporal variability in hydraulic geometry at 24 stream gaging sites in Puerto
17 Rico, and identified the watershed and river reach characteristics that correlate with each hydraulic
18 geometry parameter. These characteristics were then used to build regression models of AHG
19 parameters, with relatively high predictive power. The largest flood events from each site were
20 found to cause systematic changes to AHG parameters; most of these floods were caused by major
21 TCs. Upstream drainage area, average watershed elevation, watershed land cover and other
22 characteristics were found to be significant predictors of AHG parameters. Reaches with steeper
23 slopes were found to have limited lateral adjustability, which may reflect consolidated bank
24 materials and valley confinement. Watersheds with high percentages of forested area showed
25 greater changes in roughness but less vertical adjustability than more developed watersheds. These
26 correlation results help inform whether river channel properties in Puerto Rico and similar
27 environments are resistant to the forces of TC-induced flooding, and how these properties are
28 affected by major floods.

29 **Keywords:**

30 Hydraulic Geometry; Tropical Cyclone; Flood Hazard; Puerto Rico; Land Use

31 **Acronyms Definition:**

- 32
- 33 • AHG: At-a-station hydraulic geometry
 - 34 • TC: Tropical Cyclone
 - 35 • USGS: U.S. Geological Survey
 - 36 • NWIS: National Water Information System
 - 37 • NOAA: National Oceanic and Atmospheric Administration
 - 38 • NLS: Non-linear squares
 - 39 • WHR: median width to depth ratio
 - 40 • NACW: normalized active channel width
 - 41 • RMSE: root mean square error
 - rRMSE: relative root mean square error

42 1. Introduction

43 River cross sectional geometry is both a determinant and result of fluvial processes, including
44 flood conveyance (Guan et al., 2016; Kale & Hire, 2004), sediment transport (Bennet & Bridge,
45 1995; Bridge, 1993), riparian vegetation growth (Malkinson & Wittenberg, 2007) and channel
46 erosion (Millar & Quick, 1993; Wiman & Almstedt, 1997). At-a-station hydraulic geometry (AHG)
47 describes the relationships between discharge vs. water-surface width, mean depth, and mean
48 velocity at individual river cross sections. Power law formulations have long been used to model
49 AHG, and these formulations have been widely applied to understand river geomorphology (e.g.
50 Andreadis et al., 2013; Barefoot et al., 2019; Knighton & Wharton, 2014; Leopold et al., 1964;
51 Reid et al., 2010; Stewardson, 2005). The standard AHG formulation, which first appeared in
52 Leopold & Maddock (1953), is

$$53 \quad w = aQ^b \text{ Eqn. 1}$$

$$54 \quad d = cQ^f \text{ Eqn. 2}$$

$$55 \quad v = kQ^m \text{ Eqn. 3}$$

56 where w is channel width (typically the wetted width), d is the hydraulic depth (i.e. cross-sectional
57 area divided by w), v is mean stream velocity, and Q is the instantaneous discharge. The
58 requirement of continuity,

$$59 \quad Q = wdv = ackQ^{b+f+m} \text{ Eqn.4}$$

60 implies the constraints $ack = 1$ and $b + f + m = 1$.

61 The coefficients (a , c , and k) describe the relative magnitude of channel width, channel depth and
62 velocity (or roughness), while the exponents (b , f , and m) provide insight into how channel width,
63 channel depth and velocity change with discharge. Notwithstanding these constraints, the
64 coefficients and exponents from Eqns. 1-4 can vary substantially from place to place (Morel et al.,
65 2020b; Park, 1977), and researchers have yet to fully reveal the physical principles that underly
66 AHG behavior (Jia et al., 2017; Morel et al., 2019; not for lack of trying, e.g. Dingman, 2007;
67 Ferguson, 1986). Watershed and river reach characteristics that have been shown to explain some
68 observed AHG variability include drainage area (Qin et al., 2020), watershed orientation and

69 channel substrate (Turowski et al., 2008), suspended sediment load (Wang et al., 2006), and reach
70 slope (David et al., 2010). While recent work has built predictive models for AHG exponents (b ,
71 f , and m ; Morel et al., 2019, 2020a), the coefficients a , c , and k have received less attention (Morel
72 et al., 2020a; Qin et al., 2020; Ran et al., 2012; Turowski et al., 2008). Relationships have also
73 been shown between AHG parameters from various cross sections within individual river systems
74 (Barber & Gleason, 2018; Brinkerhoff et al., 2019; Dingman, 2007; Gleason, 2015; Gleason &
75 Smith, 2014; Turowski et al., 2008).

76 Channel morphology has also been shown to change over time due to natural processes like
77 changes in suspended sediment load (Wang et al., 2006), changing high latitude river ice regimes
78 (Best et al., 2005), floods (e.g. Hajdukiewicz et al., 2016; Magilligan et al., 2015; Sholtes et al.,
79 2018; Yochum et al., 2017), and due to human activities including urbanization (e.g. Booth, 1990;
80 Hawley et al., 2013) land cover changes (Fitzpatrick & Knox, 2000), reservoir operations (Ran et
81 al., 2012; Su et al., 2015), and sand excavation (Zhang et al., 2015). Nonetheless, analyses of
82 temporal changes in AHG and its causes remain relatively rare (Qin et al., 2020), and most existing
83 studies are confined to the mid-latitudes, while data limitations mean that AHG in more tropical
84 zones—with their unique hydroclimatic and geologic conditions—have been less studied (see
85 Lewis, 1969, Phillips & Scatena, 2013, and Turowski et al., 2008 for exceptions).

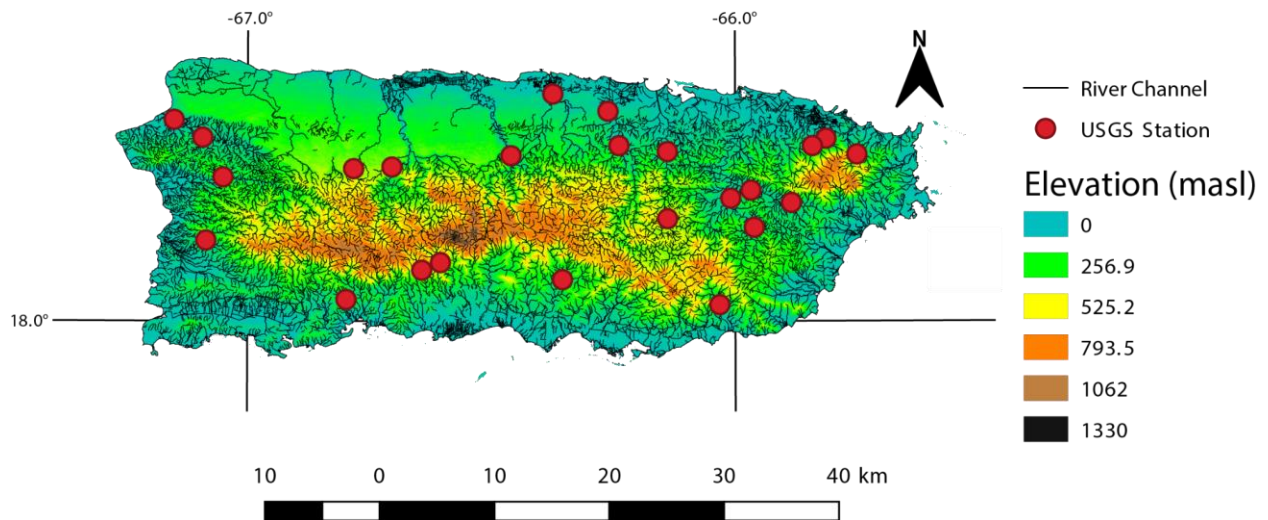
86 Tropical cyclones (TCs) hit Puerto Rico (PR) frequently and are often associated with heavy and
87 intense rainfall. This rainfall, combined with the steep mountainous terrain in PR and similar
88 environments, can produce some of the largest flood peaks per unit watershed area in the world
89 (Ogden, 2016; Smith et al., 2005). These floods can cause landslides, debris flows, mass wasting,
90 and fluvial erosion, which redistribute large amounts of sediment along the river (West et al., 2011)
91 and are capable of causing systematic lateral and vertical channel adjustments (e.g. Yousefi et al.,
92 2018). Li et al. (2020) found that channel conveyance capacity can change substantially as a result
93 of TC flooding. That study did not, however, examine how these changes manifest in terms of
94 channel geometric properties, and failed to isolate upstream watershed characteristics or local river
95 reach influence (e.g., slope, land cover) that could explain the observed conveyance capacity
96 evolution.

97 This study attempts to connect the findings of Li et al. (2020) with the AHG framework by
98 examining the watershed and river reach determinants of AHG—including whether or not it is

99 feasible to estimate AHG at ungaged sites—and also by evaluating the potential for AHG response
100 to major flood events, which are almost always caused by TCs in Puerto Rico. Such findings could
101 be valuable for applications such as simplified discharge estimation (Huang et al., 2018; Wang et
102 al., 2019): with a suitable AHG relationship between width and discharge, one can obtain
103 reasonably accurate estimates of discharge based on channel widths measured from *in-situ* or
104 remotely-sensed imagery. Identification of relevant watershed and river reach characteristics and
105 subsequent transferal to ungaged sites, meanwhile, could be used to inform flood risk management,
106 river restoration, and related actions.

107 This study examined AHG parameters for 24 sites in PR. Correlation analyses were used to identify
108 the watershed and river reach characteristics that are potentially predictive of AHG parameter
109 estimates. These characteristics were used to build multiple linear regression models for each
110 parameter, with cross validation used to evaluate their applicability to ungaged sites. Channel
111 geometry responses to TC floods were examined by calculating changes in AHG parameters after
112 major storms and comparing changes to watershed and river reach characteristics. The study region
113 and data used in this study are described in Section 2. The methodology is described in Section 3.
114 Results follow in Section 4, while discussion and conclusions are provided in Sections 5 and 6,
115 respectively.

116 2. Study Region and Data



117

118 Fig. 1: Map of Puerto Rico, showing the USGS stream gages considered in this study and elevation
119 in meters above sea level (masl; from OCM Partners, 2019). River networks (U.S. Geological
120 Survey, 2006) are shown in thin black lines.

121 Puerto Rico (PR) is a mountainous island located in the northeast Caribbean. The average elevation
122 of the mountainous middle part exceeds 1300 m above sea level (masl), while the average elevation
123 of the less steep margin is about 500 masl. Annual precipitation ranges from around 500 cm for
124 the mountainous center to 100-400 cm in the coastal lowlands (Daly et al., 2003). A monsoon
125 season begins in May and usually lasts until October, overlapping with the June-November North
126 Atlantic TC season. Limited by the island's aspect and east-west mountain range, its rivers
127 generally range from <10 kilometers to about 50 kilometers in length, with the longest—Rio de la
128 Plata—measuring 74 kilometers, and from <10 meters to more than 60 meters in width.

129 Our AHG estimation relied on field measurements of channel geometry and velocity, which the
130 US Geological Survey (USGS) performs at stream gage sites on a fairly regular basis (roughly
131 monthly) to maintain accurate rating curves, which are then used for continuous discharge
132 estimation (U.S. Geological Survey, 2021b). These field measurements were obtained from the
133 National Water Information System (NWIS) maintained by the USGS. Annual instantaneous peak
134 discharges (U.S. Geological Survey, 2021a) were used to identify the date with the largest flood
135 in each site's record.

136 We applied rigorous screening to identify suitable USGS stream gage stations. Sites with recorded
137 flags indicating influence by nearby dams, as well as those located in the vicinity of man-made
138 structures such as weirs were excluded due to their influence on AHG (Reisenbüchler et al., 2019).
139 Field measurement records in PR available through NWIS usually start around 1990, though
140 several sites' records date back to the early 1980s. If a station is reported to have experienced
141 datum changes, we avoided all observations before the most recent datum change. The site was
142 excluded from the analysis if the most recent datum change occurred later than 1990. We applied
143 the data accuracy criteria of Slater et al. (2015), who only considered field measurements in which
144 the discharge is within one percent of the product of channel velocity and cross-sectional channel
145 area, as reported by the USGS, and those made in close proximity to the gage station (within 300
146 feet [91 m]; hardly any field measurements were made directly at the gaged cross section). Only
147 sites that have continuous daily discharge records in the same period of the field measurements

148 were included. 24 sites satisfied these criteria (Fig. 1; Table S1). The limited number of sites in
149 the northwestern portion of the island is linked to the lower drainage density there.

150 Upstream watershed and river reach characteristics were obtained or estimated from public GIS
151 and remote sensing resources and used to calculate correlations with and to predict AHG
152 parameters. Watershed boundaries, along with the upstream drainage area, corresponding to each
153 stream gage were downloaded from NWIS. Watershed-averaged elevation and slope were
154 calculated for each gage based on a digital elevation model from the National Oceanic and
155 Atmospheric Administration (NOAA) National Centers for Environmental Information. We
156 matched the reach segment from the river network (U.S. Geological Survey, 2006) to each of the
157 24 gauging sites, and then measured the reach slope and sinuosity of the reach. Reach widths were
158 estimated via remote sensing imagery available through the Google Earth application. Percentages
159 of developed, forested, and planted (agricultural) areas were obtained from the USGS GAGES-II
160 dataset (Falcone, 2011). (Note that land use metrics are “static,” i.e., only available at the time
161 point when GAGES-II data were taken in 2011.)

162 **3. Methodology**

163 3.1 Hydraulic Geometry Parameter Estimation

164 To study spatial variation of the hydraulic geometry, we fit models to the entire period of field
165 measurements to get parameter estimates for each site (see black lines in Fig. 2 for examples). The
166 parameter values in Eqns. 1-3 were estimated via the nonlinear least squares (NLS) regression
167 function in the R programming language (R core team, 2020). The residuals of each NLS
168 regression model were examined for homoscedasticity, independence and normality using the
169 package “nlstools” (e.g. Fig. S1). Units used in this study are m^3/s for discharge, m for depth and
170 width, and m/s for velocity; the resulting units for a, c , and k are s/m^2 , s/m^2 and m^{-3} ,
171 respectively. Channel surface water widths and mean velocities were used to fit channel Eqns. 1
172 and 3, respectively, while hydraulic mean depths in Eqn. 2 were calculated by dividing flow areas
173 by surface water widths (after Barber & Gleason, 2018; Brinkerhoff et al., 2019; Doll et al., 2002;
174 Shen et al., 2016).

175 The fitted parameters obtained via NLS did not strictly satisfy continuity (Eqn. 4), though nearly
176 so (results not shown). We thus applied a normalization used in prior studies (Jowett, 1998; Lee et
177 al., 2019; Park, 1977) to enforce continuity (Eqn. 5 and 6):

178
$$a_{adjusted} = \frac{a_{fitted}}{(a_{fitted}c_{fitted}k_{fitted})^{\frac{1}{3}}},$$
 similar for c and k Eqn. 5

179
$$b_{adjusted} = \frac{b_{fitted}}{b_{fitted}+f_{fitted}+m_{fitted}},$$
 similar for f and m Eqn. 6.

180 We also reproduced all subsequent analyses without this normalization. Results with and without
181 normalization were nearly equivalent; results without normalization are omitted for brevity.

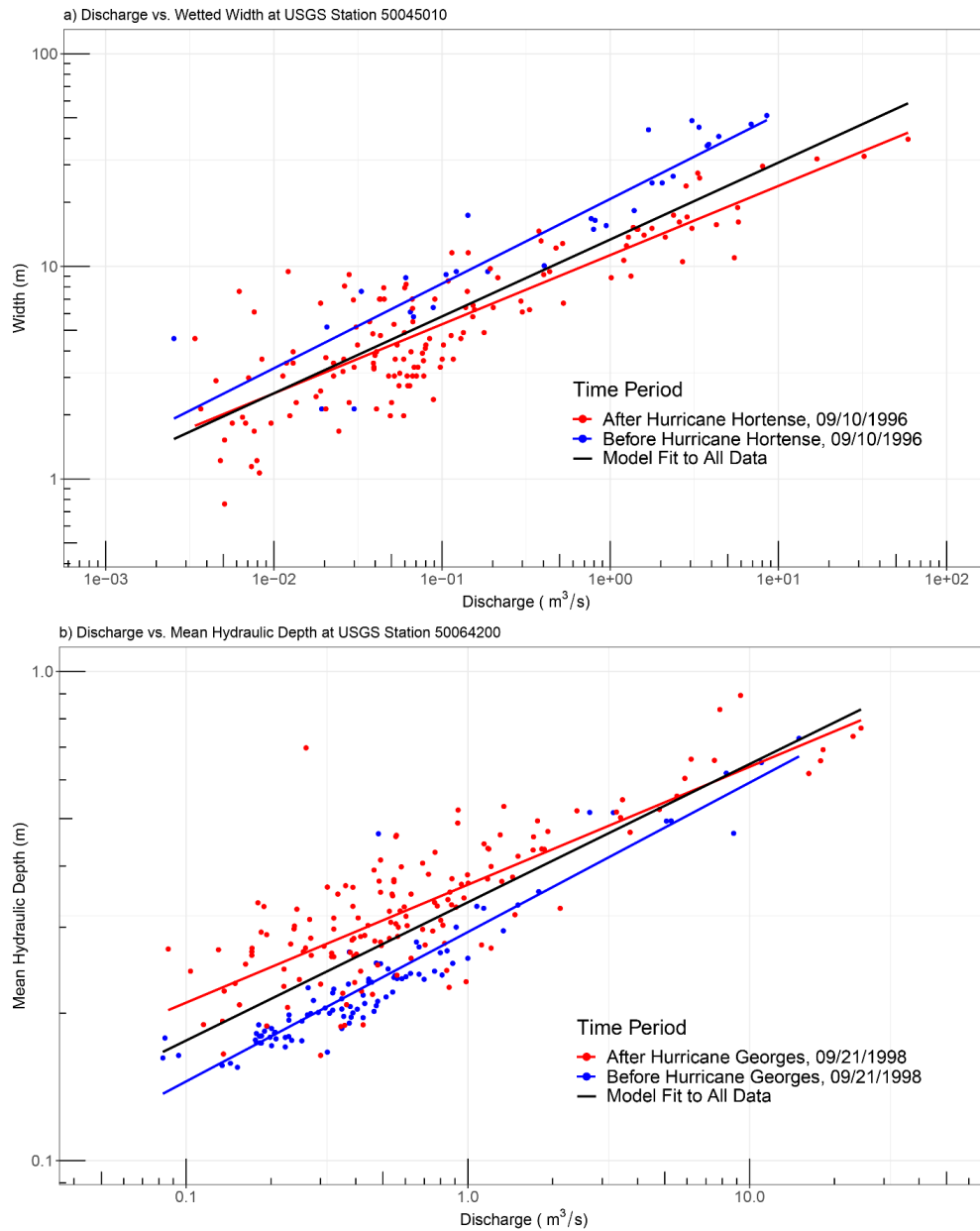
182

183 Eqns. 1 and 2 imply that channel cross-sectional geometry can be described by an equation of the
184 form

185
$$d = \frac{c}{f} w^{\frac{f}{b}}$$
 Eqn. 7

186 Eqn. 7 shows that depth is proportional to the surface water width to the power of $\frac{f}{b}$. Prior studies
187 have examined the value of $\frac{f}{b}$ as an indicator of channel cross sectional shape (Ferguson, 1986;
188 Qin et al., 2020; Turowski et al., 2008). For example, width is proportional to depth when $\frac{f}{b}=1$,
189 implying a triangular cross section while $\frac{f}{b}=2$ implies a parabolic form. When $b = 0$, $\frac{f}{b}$ would be
190 infinity, implying that the wetted width does not increase with discharge, as in cases of rectangular
191 cross section. $\frac{f}{b}<1$ represents a convex upwards curved channel section indicative of a cut
192 bank/point bar form with width increasing more than depth for medium-to-high discharges (See
193 Fig.3 in Ferguson, 1986). The ratio $\frac{c}{f}$, which indicates relative bank steepness for a particular
194 value of $\frac{f}{b}$, is absent from earlier studies. We calculated $\frac{f}{b}$ and $\frac{c}{f}$ from our AHG estimates and refer
195 to them as “bank shape parameters.”

196



200 Fig. 2 a) Discharge vs. width at site 50045010. The black line represents the fitted nonlinear least
 201 squares model using all data available at the site since 1992. The blue and red lines correspond to
 202 the model fit only to the field measurements before and after Hurricane Hortense, respectively. b)
 203 Discharge over mean depth at site 50064200. The black line represents the nonlinear least squares

204 model using all data available at the site since 1990. The blue and red lines correspond to the model
205 fit only to the field measurements before and after Hurricane Georges, respectively.

206

207 3.2 Watershed and River Reach Characteristics and Correlation Analyses

208 Upstream watershed and reach-scale characteristics were estimated to examine their relationships
209 to AHG and AHG parameter responses to floods. Other than the characteristics introduced in the
210 data section, we included three additional variables following Morel et al., (2019): Froude number
211 at median discharge of all available field measurements for each site (Fr_{50}), the median width to
212 depth ratio (WHR), and normalized active channel width ($NACW$). These are calculated as

$$213 \quad Fr_{50} = \frac{Q_{50}}{g^{0.5} H_{50}^{1.5} W_{50}} \text{ Eqn. 8}$$

$$214 \quad WHR = \frac{W_{50}}{H_{50}} \text{ Eqn. 9}$$

$$215 \quad NACW = \frac{\text{channel width}}{(\text{watershed area})^{0.42}} \text{ Eqn. 10,}$$

216 where Q_{50} , W_{50} and H_{50} are median discharge, median flow wetted width, and median depth,
217 respectively. Finally, the normalized two-year flood (calculated as the median of annual
218 instantaneous peak flows from NWIS divided by the upstream drainage area) was included to
219 describe the “peakiness” of a watershed’s flood regime. Kendall’s tau nonparametric rank
220 correlation (Kendall, 1938) was used to identify relationships between watershed/reach
221 characteristics and AHG parameters.

222 3.3 AHG predictive regression models

223 We used a stepwise process to develop models to predict AHG parameters based on watershed and
224 river reach characteristics. We began by creating multiple linear regression models for each AHG
225 parameter based on all available predictors. These were reduced to final predictive models via trial
226 and error. In order to balance model predictive power and complexity, final models were those
227 with the highest adjusted R-squared values. Some significant variables were not used in the models
228 due to collinearity among predictors. Following Morel et al. (2019), we took the natural log and
229 the square root of elevation and watershed area, respectively, before considering them as predictors.

230 To evaluate the potential predictive power of the final regression models at similar ungaged sites
231 in Puerto Rico, as well as to avoid overfitting, we performed leave-one-out cross-validation to
232 estimate the root mean square error of the predicted values of each parameter. Keeping the
233 predictors fixed, we removed one site and retrained each model with data from the other 23
234 locations. We then used the trained model to predict the parameter values for the withheld site. We
235 repeated this for all sites and then compared the predicted parameters with the observed parameter
236 values from former steps.

237

238 3.4 AHG Temporal Variation Due to Tropical Cyclones

239 Li et al. (2020) showed that recent major TCs, primarily Hurricanes Hortense (1996), Georges
240 (1998), and Maria (2017), caused substantial changes in river channel conveyance capacity in PR.
241 This earlier work, however, did little to elucidate more specific geomorphic changes. AHG
242 parameters can indeed change substantially in response to TCs (see the red and blue lines in Fig.
243 2, which show distinct AHG relationships estimated before and after major storms). We identified
244 the largest “local” flood event—the largest annual peak streamflow value for each site—to separate
245 the field measurements into two time series, before and after this largest local flood event.
246 Hurricanes Hortense and Georges caused the largest flood events at six sites each, while Hurricane
247 Maria caused the largest flood at ten others. The largest floods at the two remaining sites were
248 caused by non-TC storms. We again followed the methodology in Section 3.1 to estimate AHG
249 parameters (see Section 4.3) but only for periods four years before and four years after these
250 identified flood events. We calculated “before-and-after” percentage changes in AHG parameters
251 (including bank shape parameters) by subtracting the values after the largest flood event from the
252 values before, and dividing the difference by the latter value. These changes were then tested for
253 correlation with watershed and river reach characteristics using the nonparametric rank correlation
254 mentioned in Sec. 3.2. We extracted the peak discharges of the local largest flood events, and
255 divided them by the discharges of the 2-year flood at the same site to get normalized discharges of
256 the largest local flood events. These normalized flood discharges were included as an additional
257 characteristic in the correlation analysis specific to AHG parameter changes caused by floods.

258 **4. Results**

259 4.1 AHG Parameter Estimates and Correlation Tests

260 The power models fit reasonably well (p -values much less than 0.05) to all six parameters at all
261 sites except for velocity at site 50064200, which yielded a p -value of 0.056 (Table S2). The average
262 values for the exponents were 0.230, 0.394, and 0.376 for b , f and m , respectively. A ternary plot
263 (Fig. 3a) shows similar distributions of exponents from this study and from the earlier AHG studies
264 in Puerto Rico of Lewis (1969) and Phillips & Scatena (2013). The results are also similar to those
265 from Leopold & Maddock (1953) in the mainland midwestern United States and Leopold & Miller
266 (1956) in mainland ephemeral rivers (results not shown). Similarly to Phillips & Scatena (2013)
267 observations, we found that the width exponent is usually less than 0.33, with only one exception
268 where $b = 0.344$.

269 The relationships between AHG parameter estimates and the various watershed and reach
270 characteristics are tabulated in terms of Kendall's tau correlation (Table 1), while those of most
271 obvious interest are shown in additional ternary plots (Fig. 3b-d). Upstream watershed area was
272 found to be significantly positively (negatively) correlated with $f(m)$, while the opposite was found
273 for both percentage of developed area and planted area. Average upstream watershed elevation,
274 slope, and the percentage of forested area were found to be significant and negatively (positively)
275 correlated with $f(m)$. No characteristics were found to be significantly associated with b , and no
276 other characteristics were found to be significantly correlated with any exponents. Upstream
277 watershed area, average watershed elevation, average reach width, average reach slope, WHR,
278 Fr_{50} , and NACW were also found to be significantly correlated with some coefficients (Table 1).
279 The channel shape parameters $\frac{f}{b}$ and $\frac{a}{\frac{f}{c^b}}$ are positively and negatively correlated (at the 5% level),
280 respectively, with average watershed elevation. Upstream watershed area is also found to be
281 negatively correlated with $\frac{a}{\frac{f}{c^b}}$, while average upstream watershed slope is found to be negatively
282 correlated with $\frac{f}{b}$, both of which are significant at the 5% level.

283

284

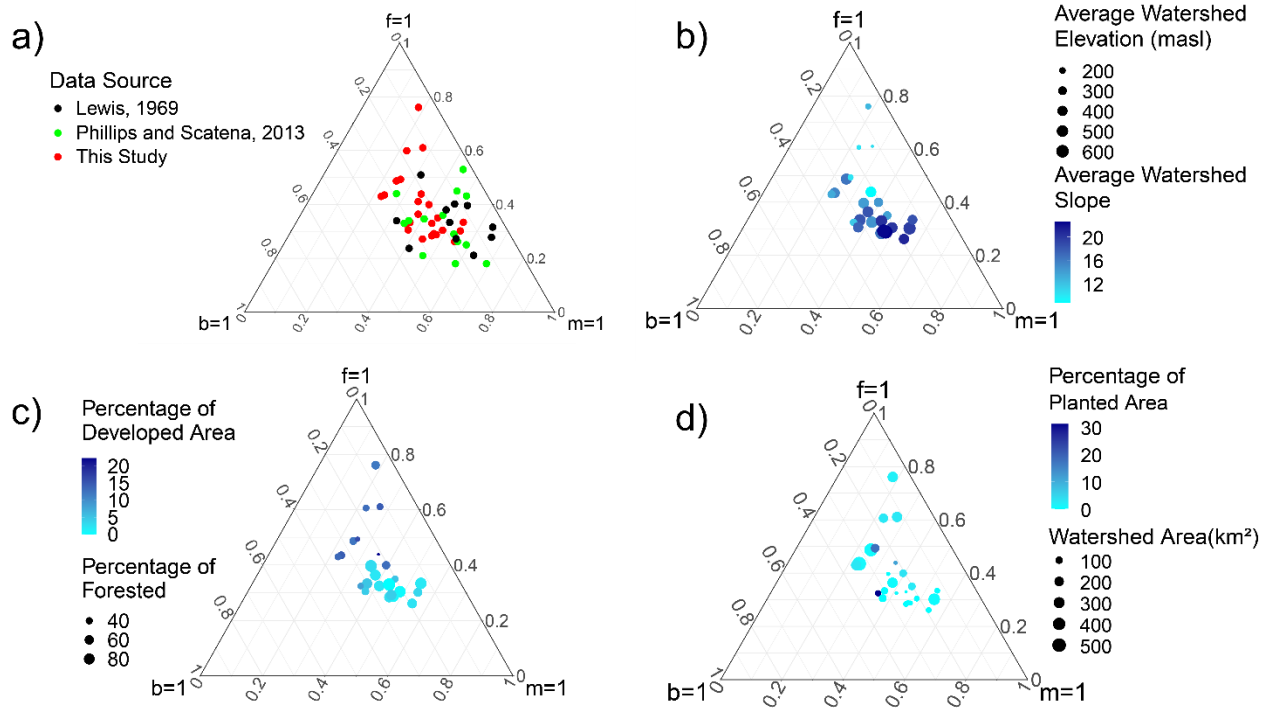
285

286 Table 1. Kendall's tau correlation results with p-values shown in parentheses. Relationships
 287 significant at the 5% level are bolded.

Watershed and River Reach Characteristics	<i>a</i>	<i>c</i>	<i>k</i>	<i>b</i>	<i>f</i>	<i>m</i>	$\frac{f}{b}$	$\frac{c}{\frac{f}{ab}}$
Normalized Two Year Flood ($\frac{m^3}{s}/km^2$)	-0.043 (0.79)	0.27 (0.07)	-0.2 (0.17)	0.17 (0.27)	-0.1 (0.51)	0.036 (0.83)	-0.14 (0.36)	0.11 (0.48)
Watershed Area (km^2)	0.48 (<0.001)	-0.5 (<0.001)	-0.062 (0.67)	-0.018 (0.9)	0.36 (0.014)	-0.36 (0.014)	0.19 (0.19)	-0.38 (0.009)
Reach width (m)	0.42 (0.004)	-0.17 (0.27)	-0.36 (0.013)	0.21 (0.16)	0.2 (0.17)	-0.25 (0.087)	0.051 (0.75)	-0.18 (0.23)
Reach slope (m/m)	-0.33 (0.023)	0.11 (0.48)	0.19 (0.21)	-0.065 (0.68)	-0.17 (0.25)	0.17 (0.27)	-0.11 (0.48)	0.22 (0.13)
Watershed Forested Area (%)	-0.029 (0.86)	0.27 (0.07)	-0.25 (0.097)	-0.094 (0.54)	-0.3 (0.039)	0.38 (0.008)	-0.094 (0.54)	0.094 (0.54)
Watershed Developed Area (%)	0.08 (0.61)	-0.23 (0.12)	0.25 (0.087)	0.087 (0.57)	0.51 (<0.001)	-0.51 (<0.001)	0.22 (0.14)	-0.19 (0.21)
Watershed Planted Area (%)	0.11 (0.47)	-0.13 (0.39)	0.093 (0.54)	0.07 (0.65)	0.49 (0.001)	-0.44 (0.004)	0.26 (0.092)	-0.23 (0.14)
Average watershed slope	-0.072 (0.64)	0.15 (0.31)	-0.23 (0.12)	0.007 (0.98)	-0.57 (<0.001)	0.54 (<0.001)	-0.31 (0.034)	0.22 (0.13)
Average watershed elevation (masl)	-0.17 (0.25)	0.3 (0.044)	-0.22 (0.14)	0.15 (0.31)	-0.49 (<0.001)	0.41 (0.004)	-0.36 (0.015)	0.41 (0.004)
WHR	0.2 (0.17)	-0.33 (0.026)	-0.13 (0.39)	-0.2 (0.19)	-0.26 (0.078)	0.27 (0.07)	-0.094 (0.54)	-0.094 (0.54)
Fr_{50}	0.21 (0.16)	-0.39 (0.007)	0.12 (0.42)	0.087 (0.57)	0.21 (0.16)	-0.28 (0.062)	-0.043 (0.79)	-0.058 (0.71)
NACW (m)	0.16 (0.29)	0.065 (0.68)	-0.38 (0.010)	0.27 (0.07)	-0.043 (0.79)	-0.065 (0.68)	-0.14 (0.36)	0.065 (0.68)
Sinuosity (m/m)	0.094 (0.54)	0 (1)	0.022 (0.9)	-0.058 (0.71)	0.065 (0.68)	-0.014 (0.94)	0.043 (0.79)	-0.014 (0.94)

288

289

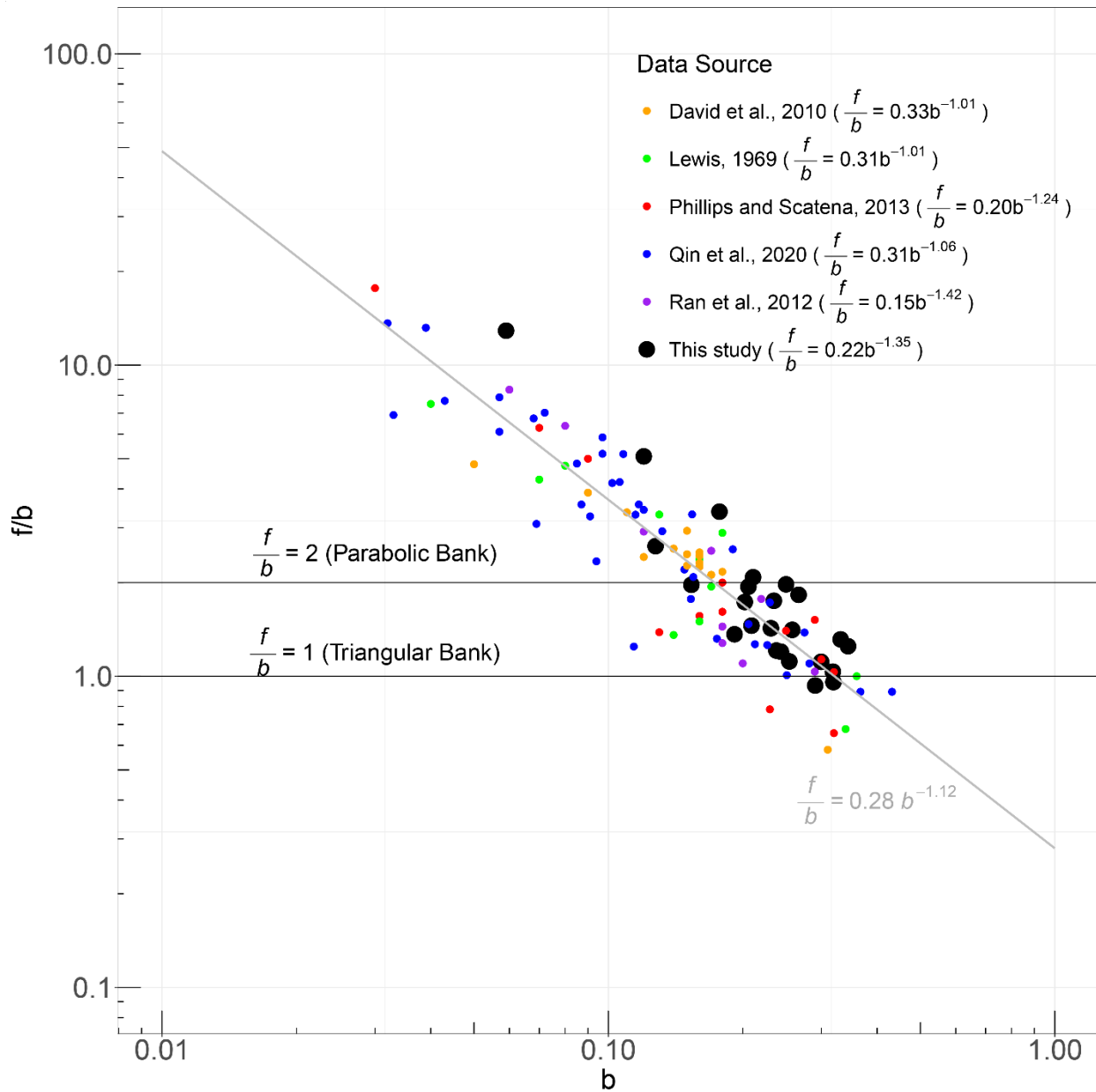


290

291 Fig. 3: Ternary plots showing the estimated exponents for the entire study period: a) Comparison
 292 to former studies in Puerto Rico, b) relationships with average watershed slope and elevation, c)
 293 relationships with percentages of developed and forested area, and d) relationships with percentage
 294 of planted area and watershed area.

295 The ratio $\frac{f}{b}$ was found to be negatively correlated ($p=0.023$) with average watershed elevation,
 296 indicating that higher-elevation rivers in PR tend toward more triangular and less rectangular
 297 channel cross-sectional shapes. Turowski et al. (2008) found a strong log-log relationship between
 298 the bank shape parameter $\frac{f}{b}$ and the exponent b for average parameter values in different studies.
 299 By comparing our data with prior studies, we found that this relationship appears to hold across a
 300 wide range of studies and study locations. The range of coefficients of the models fit separately to
 301 each of the five studies shown on this plot is 0.15 - 0.33. The range of exponents is -1.42 - -1.01.
 302 The coefficient and exponent of the model fit to our data are 0.22 and -1.35, respectively, which
 303 are within the range. The model fit range also contains the equation in Turowski et al. (2008; Fig.
 304 4, gray line; $\frac{f}{b} = (0.28 \pm 0.06)b^{-1.12 \pm 0.07}$). This confirms that in Puerto Rico, as in other locations,
 305 general, steep-banked channels lead to smaller exponent b , which is indicative of width being less

306 adjustable, which can be caused by consolidated bank materials like cohesive soils that are
307 common in cases of steep banks.



308

309 Fig. 4 Scatterplot of f/b vs. b using data from multiple former studies and this study. All model
310 fits are significant (p -values $< 10^{-3}$) Gray line shows the model fit by Turowski et al. (2008), to
311 multiple studies. The model from Turowski et al. (2008) was fit to average values of each study,
312 rather than whole data sets from the studies. The only common study between the five former
313 studies shown on this plot and the studies analyzed in Turowski et al. (2008) is Lewis (1969).

314 4.2 AHG Predictive Models

315 The final regression models to predict AHG parameters (Section 3.3) are shown in Table 2, along
 316 with R-squared values and overall model p-values. Among the three coefficients (exponents), $k(b)$
 317 is least well predicted, in terms of adjusted R-squared. The regression model for b is the only
 318 model that is insignificant at 5% level. When subject to leave-one-out cross validation, all
 319 regression-based models can predict parameter values with relative root mean square error
 320 (rRMSE; RMSE divided by the average parameter value) between 10% and 30%, except for the
 321 model for b , which results in 31.2%.

322 Table 2. Regression-based predictive models for AHG parameters. Predictors are: width to depth
 323 ratio at median discharge (WHR), average watershed slope (S_{ws}), average watershed elevation
 324 ($Elev_{ws}$), watershed area (A_{ws}), the percentages of developed area ($Developed$), forested area
 325 ($Forested$) and planted area ($Planted$), normalized two year flood (Q_{2yr}), reach slope (S_r), reach
 326 sinuosity ($sinuosity$), channel width (w_c), normalized active channel width ($NACW$) and Froude
 327 number at median discharge (Fr_{50}). In the leave-one-out validation, models were repeatedly fit to
 328 23 sites, and then used to predict the remaining site’s parameter. RMSEs were calculated between
 329 the leave-one-out predictions estimated values shown in Table S2; units match those of the
 330 corresponding AHG parameter. Relative RMSEs were calculated by normalizing RMSEs by the
 331 mean parameter value from Table S2 and multiplying by 100.

Model Structure	Adjusted R^2	R^2	p-value	Leave-one-out RMSE (Relative RMSE)
$a = -1.97 + 0.11WHR + 0.53\sqrt{A_{ws}} + 0.066Forested$	0.83	0.85	<0.001	3.3 (25.7%)
$c = -0.36 + 0.10\log(Elev_{ws}) + 0.0039Planted + 0.0074Q_{2yr}$	0.55	0.61	<0.001	0.048 (18.3%)
$k = 0.66 - 0.010S_{ws} - 0.039NACW - 0.0039\sqrt{A_{ws}}$	0.38	0.46	0.007	0.095 (28.2%)
$b = -0.20 - 7.6e - 04WHR + 0.095\log(Elev_{ws}) - 0.0015Forested$	0.18	0.29	0.08	0.072 (31.2%)
$f = 1.18 + 0.0033Forested + 0.015Developed - 0.18\log(Elev_{ws})$	0.67	0.71	<0.001	0.073 (18.5%)
$m = 0.22 + 0.013S_{ws} - 0.010\sqrt{A_{ws}} + 0.0013WHR$	0.76	0.79	<0.001	0.060 (15.9%)

332

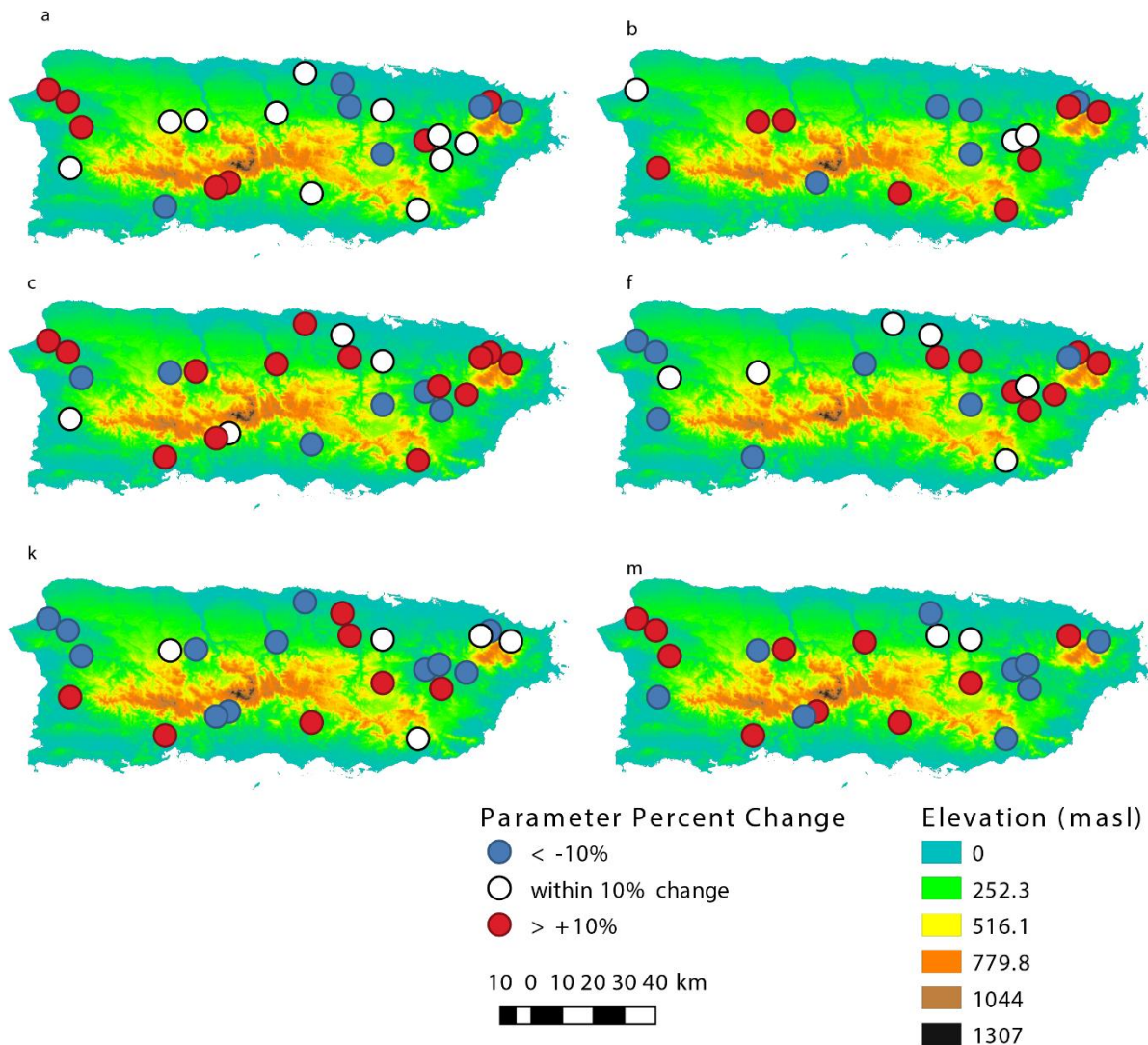
333 4.3 Hydraulic Geometry Response to Tropical Cyclones

334 We re-estimated AHG parameters for each site using two periods: four years before and after the
335 largest local flood event (i.e., the highest single instantaneous flood peak for each site, see Sec.3.4).
336 Both the percent differences between the “before-and-after” parameter values and the absolute
337 value of these differences were calculated. The absolute values are generally indicative of the
338 overall tendency of a site’s AHG relations to change in response to a major flood, while the real
339 difference provides the direction of that change. The differences in the parameter values of the
340 largest local flood event are shown in Fig. 5. Percent changes in parameter values are evident at
341 most sites and for all parameters. The changes in the depth exponent f tend to be positive in the
342 northeastern part of the island and negative in western Puerto Rico. No obvious spatial patterns
343 were evident for other parameters.

344 We then computed correlations between these parameter value changes and the various watershed
345 and river reach characteristics (Table 3). Froude number, sinuosity, and NACW are positively and
346 significantly (at 5% level) correlated with the real percent difference of a , while NACW is also
347 negatively correlated ($p=0.034$) with the real percent difference in k . Normalized two-year flood
348 and WHR are positively correlated with the shape coefficient $\frac{c}{\frac{f}{ab}}$ (p -values are 0.042 and 0.03,
349 respectively). The percentage of forested (developed) area is negatively (positively) correlated
350 with the absolute percent difference of k , with p -values of 0.03 (0.008). The percentage of forested
351 (developed) area is also positively (negatively) correlated with the absolute percent difference of
352 b , with p -values of 0.003 (0.009) . Watershed area, reach width, and the percentage of planted area
353 are also significantly negatively correlated with the absolute percent difference of b . The
354 percentage of planted area (average watershed slope) is positively (negatively) correlated with the
355 absolute percent change of c , with $p=0.036$ ($p=0.017$).

356

357



358

359 Fig. 5. Real percent parameter value changes of the largest flood event for all AHG parameters.
 360 Only the sites with significant model estimates for both before and after the largest flood event are
 361 shown on each panel. Number of sites shown on each panel: 24 for coefficients (*a*, *c* and *k*), 16
 362 for *b*, 20 for *f*, and 21 for *m*. Blue dots are the sites with real parameter value decreases greater
 363 than 10%, while red dots are the sites with real parameter value increases greater than 10%. White
 364 dots are the sites within between 10% decreases and 10% increases.

365 Table 3. Kendall's Tau correlation test results of percent parameter changes caused by the largest
 366 local flood event and watershed/river reach characteristics. The values outside of the brackets are
 367 the correlations entry between the predictor and the percent parameter change, while the values

368 inside brackets are the correlations between the predictor and the absolute value of the percent
 369 parameter change. Quantities inside parentheses are corresponding p-values; bolded results are
 370 significant at the 5% level.

Watershed and River Reach Characteristics	<i>a</i> (N=24)	<i>c</i> (N=24)	<i>k</i> (N=24)	<i>b</i> (N=16)	<i>f</i> (N=20)	<i>m</i> (N=21)	$\frac{f}{b}$ (N=13)	$\frac{c}{\frac{f}{ab}}$ (N=13)
Normalized Two Year Flood ($\frac{m^3}{s}/km^2$)	0.16 (0.29) 0.16 (0.29)	0.17 (0.25) 0.087 (0.57)	-0.27 (0.07) -0.087 (0.57)	0.23 (0.23) 0.083 (0.69)	0.032 (0.87) -0.063 (0.72)	-0.17 (0.29) -0.24 (0.14)	-0.18 (0.44) -0.23 (0.31)	0.44 (0.042) 0.15 (0.51)
Watershed Area (km^2)	0.083 (0.57) -0.098 (0.5)	-0.025 (0.86) 0.12 (0.41)	0.0036 (0.98) 0.19 (0.21)	-0.21 (0.26) -0.49 (0.0078)	0.1 (0.54) 0.037 (0.82)	0.072 (0.65) 0.11 (0.49)	0.25 (0.25) -0.09 (0.67)	-0.37 (0.076) -0.039 (0.85)
Reach width (m)	0.28 (0.062) 0.072 (0.64)	0.13 (0.39) 0.22 (0.14)	-0.25 (0.087) 0.087 (0.57)	-0.22 (0.27) -0.4 (0.033)	0.22 (0.19) 0.021 (0.92)	-0.038 (0.83) -0.029 (0.88)	0.31 (0.16) -0.15 (0.51)	-0.26 (0.25) 0.23 (0.31)
Reach slope (m/m)	-0.043 (0.79) 0.029 (0.86)	0 (1) -0.13 (0.39)	-0.022 (0.9) -0.14 (0.34)	0.067 (0.76) 0.22 (0.27)	-0.084 (0.63) 0.16 (0.35)	0.086 (0.61) -0.15 (0.35)	-0.1 (0.68) 0.36 (0.1)	0.1 (0.68) 0.18 (0.44)
Watershed Forested Area (%)	0.014 (0.94) 0.12 (0.45)	0.058 (0.71) -0.23 (0.12)	-0.12 (0.42) -0.32 (0.03)	0.22 (0.27) 0.53 (0.0033)	-0.063 (0.72) -0.14 (0.42)	-0.067 (0.7) -0.13 (0.42)	-0.23 (0.31) 0.23 (0.31)	0.18 (0.44) 0.1 (0.68)
Watershed Developed Area (%)	0.036 (0.83) -0.065 (0.68)	0.0072 (0.98) 0.25 (0.087)	0.014 (0.94) 0.38 (0.0082)	-0.37 (0.052) -0.48 (0.0086)	0.074 (0.68) 0.084 (0.63)	0.019 (0.93) 0.1 (0.53)	0.36 (0.1) 0 (1)	-0.31 (0.16) -0.026 (0.95)
Watershed Planted Area (%)	0.039 (0.8) -0.078 (0.61)	0.093 (0.54) 0.32 (0.036)	-0.031 (0.84) 0.18 (0.24)	-0.27 (0.17) -0.45 (0.021)	0.17 (0.31) 0.17 (0.31)	0 (1) 0.01 (0.95)	0.27 (0.21) -0.11 (0.61)	-0.19 (0.38) -0.055 (0.8)
Average watershed slope	-0.1 (0.51) 0.029 (0.86)	-0.058 (0.71) -0.35 (0.017)	0.065 (0.68) -0.26 (0.078)	0.32 (0.096) 0.33 (0.079)	-0.053 (0.77) -0.021 (0.92)	0.0095 (0.98) 0.076 (0.65)	-0.31 (0.16) 0 (1)	0.21 (0.37) 0.077 (0.77)
Average watershed elevation (masl)	-0.072 (0.64) 0.072 (0.64)	-0.014 (0.94) -0.19 (0.21)	0.065 (0.68) -0.13 (0.39)	0.05 (0.82) 0.27 (0.17)	0 (1) -0.14 (0.42)	0 (1) -0.0095 (0.98)	-0.051 (0.86) 0.051 (0.86)	0.21 (0.37) 0.28 (0.2)
WHR	0.31 (0.034) 0.036 (0.83)	0.11 (0.48) 0.17 (0.27)	-0.28 (0.062) 0.094 (0.54)	-0.067 (0.76) 0.15 (0.45)	-0.16 (0.35) -0.23 (0.16)	0.057 (0.74) 0.12 (0.46)	-0.21 (0.37) 0.051 (0.86)	0.21 (0.37) -0.13 (0.59)
Fr_{50}	0.072 (0.64) -0.28 (0.062)	0.014 (0.94) 0.029 (0.86)	-0.065 (0.68) -0.12 (0.45)	0.2 (0.31) -0.017 (0.96)	-0.032 (0.87) 0.13 (0.46)	0.22 (0.18) 0.25 (0.12)	-0.26 (0.25) -0.31 (0.16)	0.46 (0.03) -0.13 (0.59)
NACW (m)	0.31 (0.034) -0.0072 (0.98)	0.065 (0.68) 0.14 (0.36)	-0.28 (0.062) 0.18 (0.23)	0.033 (0.89) -0.15 (0.45)	0.084 (0.63) -0.18 (0.29)	-0.14 (0.39) 0.19 (0.24)	0.026 (0.95) -0.13 (0.59)	-0.18 (0.44) -0.21 (0.37)
Sinuosity (m/m)	0.3 (0.039) 0.16 (0.29)	0.12 (0.45) 0.23 (0.12)	-0.31 (0.034) 0.014 (0.94)	-0.22 (0.27) -0.067 (0.76)	0.15 (0.39) -0.053 (0.77)	0.0095 (0.98) 0 (1)	0.26 (0.25) -0.051 (0.86)	0 (1) 0.28 (0.2)
$\frac{Q_{largest}}{Q_{2yr}}$	-0.14 (0.34) -0.22 (0.14)	-0.17 (0.25) -0.1 (0.51)	0.21 (0.16) 0 (1)	-0.1 (0.63) 0.083 (0.69)	-0.15 (0.39) -0.011 (0.97)	0.2 (0.22) 0.11 (0.49)	-0.051 (0.86) 0.21 (0.37)	-0.21 (0.37) -0.28 (0.2)

371

372 5. Discussion

373 5.1 Comparison with other studies

374 The average values of the exponents b , f , m obtained in this study are 0.230, 0.394 and 0.376,
375 respectively, which are close to Lewis (1969) and Phillips & Scatena (2013) results in Puerto Rico
376 (Fig. 3a), Leopold and Maddock's results in the Midwest US (Leopold & Maddock, 1953), and
377 Leopold and Miller's results in ephemeral streams in US (Leopold & Miller, 1956). The b and
378 f values agree with the prior work in Puerto Rico (Phillips & Scatena 2013) in that width (b)
379 contributes a smaller component than depth (f) and velocity (m), and never exceeds one third (with
380 only one minor exception; one site's value of b is 0.34). In 14 sites, velocity has the largest
381 exponent, while depth has the largest exponent in the other 10 sites. Width never had the largest
382 exponent, similar to Qin et al. (2020).

383 The ratio $\frac{f}{b}$ describes the shape of river banks (Ferguson, 1986), ranging from 0.93 to 12.89 in this
384 study, with the median of 1.44. The majority of sites have ratios within or near the range 1-2,
385 indicating that the majority of channel cross sections are either triangular or parabolic. The ratio
386 at some sites, however, are higher, highlighting that there does exist a diversity of channel cross-
387 sectional shapes in Puerto Rico including ones closer to rectangular.

388 The log-log linear relationship between the shape parameter $\frac{f}{b}$ and b are significant for both our
389 data and a collection of parameters from former studies conducted in Puerto Rico, Colorado in the
390 mountainous western United States, and the Yellow River in China. The fitted equations are all
391 close to what Turowski et al. (2008) found using average values from other studies. Despite the
392 strong log-log relationship between $\frac{f}{b}$ and b , we found that this relationship did not predict b as
393 well as the regression-based model for that parameter (see Table 2; RMSE and rRMSE of b
394 estimates based on the log-linear model are 0.61 and 265%). This may be due to the requisite log
395 and exponential transformations. Nonetheless, the high similarity of the log-log linear relationship
396 among different studies in highly varied geographic regions suggests the potential to estimate
397 channel shape from the exponent b .

398

399 5.2 Hydraulic parameters and watershed and river reach characteristics

400 5.2.1 Exponents

401 The characteristics that were significantly correlated with the depth exponent f were inversely
402 correlated with the velocity exponent m (Table 1), which is not unexpected due to the continuity
403 requirement (Eqn. 4). These characteristics include upstream drainage area, the percentages of
404 developed, forested and planted area, average upstream watershed slope and elevation. Our results
405 are consistent with Klein (1981) and Qin et al. (2020), in that depth is a greater contributor for
406 higher discharges in large rivers (positive correlation between watershed area and f), while width
407 contributes more in small streams (negative—but not statistically significant—correlation between
408 upstream watershed area and b). No watershed or river reach characteristics were found to be
409 significantly (i.e. at the 5% level) correlated with the width exponent b .

410 Phillips and Scatena (2013) found that while velocity has a larger exponent for rural channels in
411 Puerto Rico, depth contributes to a larger exponent extent in urban catchments. Our correlation
412 results agree with this finding: the percentage of developed (forested) area of a watershed is
413 positively (negatively) correlated with the depth exponent f and negatively (positively) with the
414 velocity exponent m . This is further supported by the significant and positive correlation between
415 $f - m$ and percentage of developed area (Kendall's tau = 0.54, $p=10^{-4}$). Cohesive banks are
416 common in both developed and forested watersheds; with stable banks, the river channels have
417 limited lateral adjustability (Millar and Quick, 1993; Millar, 2000). This potentially explains why
418 land cover metrics were not significantly correlated with b . The positive correlation between f
419 and the percentage of developed area indicates that the channels tend to adjust vertically in more
420 developed watersheds than in more forested watersheds, which agrees with previous research
421 showing that channels in urbanized environments are often prone to incision (Booth, 1990; Cole
422 et al., 2017). In forested watersheds, wood load can contribute to flow resistance and is subject to
423 adjustments from frequent and flashy floods (Cadol and Wohl, 2013), in support of the positive
424 correlation between m (adjustability of channel roughness) and percent forested area.

425 The average elevation and slope of the watersheds are highly correlated (Kendall's tau=0.58; $p<10^{-4}$)
426 ⁴), and thus yield similar correlations with f (negative) and m (positive). Ran et al. (2012) and
427 others have concluded that mountainous bedrock channels are typically stable, meaning scour and
428 infill are negligible. This likely explains our result that higher-elevation and steeper (i.e. more
429 mountainous) watersheds accommodate increasing discharge primarily through velocity (positive
430 correlation with m) rather than depth (negative correlation with f).

431

432 5.2.2 Coefficients and bank shape parameters

433 Average watershed elevation was found to be negatively correlated with $\frac{f}{b}$ (Kendall's tau: -0.33,
434 $p=0.023$; Table 4) and positively correlated with $\frac{c}{ab}$. Since most channels have forms between
435 triangular ($\frac{f}{b} = 1$) and parabolic ($\frac{f}{b} = 2$), this correlation suggests that lower-elevation channels
436 tend to be parabolic with a gradually-sloped banks, while the higher-elevation channels tend to be
437 triangular with steeper banks. This can be explained by the difference of channel substrate: higher-
438 elevation watersheds are usually in mountainous areas with bedrock channels, while rivers in
439 lower-elevation areas carry more alluvium which can be “shaped” into parabolic forms (Ran et al.,
440 2012).

441 The coefficients in Eqns. 1-3 are unit-dependent, and are usually treated as values of width, depth
442 or velocity when the discharge equals one unit (m^3/s in our case; Dingman & Afshari, 2018). The
443 coefficients are general indicators of a channel's width, depth, and roughness. How these
444 characteristics influence discharges at different flow levels is determined by exponents. For
445 example, in Ran et al., 2012, a wide channel with highly-cohesive steep banks result in a high
446 value of a and a relatively small value of b .

447 Upstream drainage area was significantly correlated with a (positive) and c (negative), and
448 negatively but insignificantly correlated with k . This is similar to Qin et al. (2020), and suggests
449 that channels in the larger watersheds in Puerto Rico are generally more “wide” than “deep,” in
450 terms of cross-sectional geometric controls on discharge. Reach width is significantly and
451 positively correlated with a , confirming the interpretation of a as a scale factor for channel width
452 (Ran et al., 2012). The significant positive correlation between reach width and k can be explained
453 by continuity (Eqn. 4). Reach slope is found to be negatively significantly correlated with a , in
454 support of that channels with greater slope have lower width to depth ratios due to less lateral
455 adjustability of resistant bank material. The significant positive correlation between average
456 watershed elevation and c shows that mountainous channels in Puerto Rico are usually deep,
457 consistent with the observation mentioned above that channels at high elevations are more likely
458 to be triangular rather than parabolic. High values of normalized active channel width reflect wide

459 channels relative to catchment size (by Eqn. 7; Morel et al., 2019), which could be indicative of
460 increases in roughness associated with feedbacks between channel width and instream wood
461 loading (negative correlation between normalized active channel width and k ; Table 1), agreeing
462 with former studies in that wood load increases flow resistance (Cadot & Wohl, 2013; Curran &
463 Hession, 2013; McBride et al., 2007; McBride et al., 2008).

464 Coefficients are more influential when values of the variable (width, depth and velocity) are low,
465 while exponents are more influential for high values. To demonstrate, we considered AHG
466 parameters together with published flood stages obtained from National Weather Service (National
467 Oceanic and Atmospheric Administration, 2021) to predict bankfull discharges based on Eqn. 2.
468 We found that on average, exponents are more influential than coefficients at determining bankfull
469 discharge at flood stage. For example, a 1% increase in f can result in an average decrease in
470 bankfull discharge of 7.1%, while a 1% increase in c gave only an average decrease of 2.9%. It
471 should be noted, however, that few sites have direct discharge measurements near or above these
472 flood stages (see also Li et al. 2020 for discussion on this and other limitations in the PR field
473 measurements), so these results should be taken with a grain of salt. This calls for further data to
474 better understand the influence of both coefficients and exponents at flood discharges.

475

476 5.3 Predictive Models

477 The leave-one-out estimates reach an acceptable level of accuracy suggested by the relative RMSE.
478 The root mean square errors (relative RMSEs) for estimates of b , f and m are 0.072 (31.16%),
479 0.073 (18.48%), and 0.060 (15.94%) [-], respectively. The RMSE and p-values are generally lower,
480 and R-squared values generally higher, than Morel's models (Morel et al., 2019), likely due to a
481 much reduced geographic scope and thus a smaller, more homogeneous set of sites. The RMSE
482 (relative RMSE) for coefficients a , c and k are 3.3 s/m² (25.67%), 0.048 s/m² (18.26%) and 0.095
483 m⁻² (28.18%), respectively. The high root mean square of a is due to its wide range and much
484 higher magnitude compared to other parameters. The regression models not only yielded reliable
485 estimates of the parameters at the study sites, but show the potential to predict parameter values
486 for ungaged sites in similar environmental settings.

487 5.4 Tropical Cyclone Effects on AHG

488 The normalized two-year flood is positively correlated with real (i.e., not absolute) percent change
489 of $\frac{c}{F}$, indicating that greater “flashiness” can steepen shapes after floods, possibly as a result of
490 channel incision (e.g., Schumm et al. 1984; Simon & Rinaldi 2006; Wallerstein & Thorne, 2004).
491 WHR is also positively correlated with real percent change of $\frac{c}{F}$, which shows that banks in
492 channels with flatter cross-sections erode more readily than channels with steep banks, which is
493 likely indicative of constraints on lateral adjustability imposed by consolidated or cohesive bank
494 materials, or vegetative root reinforcement ([Millar and Quick, 1993](#); [Millar, 2000](#)). Sinuosity, F_{50} ,
495 and NACW are positively correlated with the real percent change of a , showing that in meandering
496 and wide channels and in channels with high F_{50} , channel widths tend to increase after floods. This
497 is consistent with the expectation that sinuous channels are fully alluvial with laterally adjustable
498 channel boundaries. The negative correlation between NACW and real percent change of k is
499 probably caused by continuity requirement (Eqn. 4).

500 Average watershed slope is found to be negatively correlated with absolute percent change of c ,
501 consistent with the observation from section 5.2 that rivers in steeper watersheds are more stable.
502 This agrees with former research that rivers in mountainous areas are usually supply limited and
503 have resistant boundaries that are less responsive to changing in driving forces (Montgomery &
504 Buffington, 1997; Montgomery & MacDonald, 2002). Reach width and watershed area are
505 negatively correlated with absolute change of b , showing that channel width’s contribution to
506 discharge is relatively more (less) stable in the larger (smaller) study watersheds and wider
507 (narrower) channels, agreeing with Qin et al. (2020) that river stability tends to increase with
508 watershed area. The percentage of developed (forested) area is positively (negatively) correlated
509 with the absolute change k , indicating that flow velocity is relatively more stable in forested
510 watersheds than in urban channels facing TC floods. Flow velocities in locations with vegetated
511 banks and large in-stream roughness elements tend to be confined to narrower ranges (Zong and
512 Nepf, 2010; Curran & Hession, 2013), thus we would expect flow velocities to experience less
513 change in forested areas than in more developed areas. The percentage of developed (forested)
514 area is negatively (positively) correlated with the absolute change of b , showing that the lateral
515 adjustability is more stable in developed watersheds than in forested ones. This makes sense since

516 urban channels are often anthropogenically confined. More data on channel boundary materials
517 and vegetation could help future study analyze the stability of the river channels in Puerto Rico.

518 Li et al. (2020) found that river channels can experience both significant instant and gradual
519 changes as responses to floods brought by TCs from a broader view focusing on channel
520 conveyance capacity. How these conveyance capacity changes were achieved by river reaches,
521 however, was not discussed in that paper. We herein elaborated on how channels adjust their
522 geometry and roughness—changes of which can result in conveyance capacity changes—and
523 identified potential predictors that render the channel geometry and roughness changes brought by
524 TC floods more qualitatively predictable. Future studies on the quantitative connections between
525 AHG parameter changes and conveyance capacity change are suggested; potentially applying
526 AHG parameter regression models to conveyance capacity estimation. This could provide practical
527 information for flood hazard management in dynamic channel networks.

528 529 **6. Summary and Conclusions**

530
531 River cross sectional geometry plays a critical role in fluvial processes (e.g. (Bennet & Bridge,
532 1995; Guan et al., 2016; Malkinson & Wittenberg, 2007). Power law at-a-station hydraulic
533 geometry (AHG) formulations describing this geometry were introduced more than 60 years ago
534 (Leopold & Maddock, 1953) and have been widely confirmed empirically and analyzed
535 theoretically (e.g. (Andreadis et al., 2013; Barefoot et al., 2019; Dingman, 2007; Ferguson, 1986).
536 The physical controls of AHG remain underexplored (Jia et al., 2017; Qin et al., 2020), however,
537 especially in tropical areas which are generally less instrumented than more temperate zones.

538 In Puerto Rico, the intense precipitation brought by tropical cyclones (TCs) has been shown before
539 to cause substantial changes to channel conveyance capacity via sediment redistribution (Li et al.,
540 2020). That study failed to identify the mechanisms for such changes, however. In this study, we
541 examine AHG at 24 stream gage sites in Puerto Rico, with a focus on understanding and modeling
542 the upstream and river reach controls on AHG—with one goal being AHG estimation at ungaged
543 sites—as well as how AHG can respond to major TC-induced floods. Key findings and conclusions
544 are summarized here:

- 545 1. AHG parameters are highly correlated with a range of watershed and river reach
546 characteristics; these relationships can largely be understood through existing
547 geomorphological reasoning. AHG parameter estimates in this study are similar in
548 magnitude to former studies in Puerto Rico.
- 549 2. AHG parameters can be robustly predicted using multiple linear regression with watershed
550 and river reach characteristics. We can reach acceptable accuracy (relative RMSEs are
551 usually between 10% and 30%) using these models, which could be used to predict AHG
552 parameters in similar settings where cross sectional geometry data are lacking.
- 553 3. Some sites showed distinct changes in AHG—such as narrowed and deepened channels—
554 after large floods, the large majority of which were caused by TCs. Certain watershed and
555 river reach characteristics, specifically upstream watershed area, average watershed slope,
556 watershed land cover, reach width, WHR, NACW, and sinuosity, are predictive both of
557 whether and how AHG parameters change in response to floods.

558 **Acknowledgments**

559 Y. Li's contributions were supported by the Wisconsin Alumni Research Foundation.

560 **Data Availability Statement**

561 Field measurements, daily discharge records, site locations, and watershed shapefiles for all stream
562 gaging sites available through U.S. Geological Survey NWIS system (U.S. Geological Survey,
563 2021a, 2021b). River network shapefile is available through U.S. Geological Survey, National
564 Hydrography Dataset (U.S. Geological Survey, 2006). Percentages of developed area and forested
565 area are available through the GAGES II data set (Falcone, 2011). The list of TCs that affected
566 Puerto Rico during the study period is available through the HURDAT-2 data set (Landsea &
567 Franklin, 2013). The digital elevation model is available through OCM Partners (2019). Codes
568 used for analyses are available from the corresponding author.

569

570 **References**

571 Andreadis, K. M., Schumann, G. J.-P., & Pavelsky, T. (2013). A simple global river bankfull width and
572 depth database: Data and Analysis Note. *Water Resources Research*, 49(10), 7164–7168.
573 <https://doi.org/10.1002/wrcr.20440>

574 Barber, C. A., & Gleason, C. J. (2018). Verifying the prevalence, properties, and congruent hydraulics of
575 at-many-stations hydraulic geometry (AMHG) for rivers in the continental United States. *Journal*
576 *of Hydrology*, 556, 625–633. <https://doi.org/10.1016/j.jhydrol.2017.11.038>

577 Barefoot, E., Pavelsky, T. M., Allen, G. H., Zimmer, M. A., & McGlynn, B. L. (2019). Temporally Variable
578 Stream Width and Surface Area Distributions in a Headwater Catchment. *Water Resources*
579 *Research*, 55(8), 7166–7181. <https://doi.org/10.1029/2018WR023877>

580 Bennet, S. J., & Bridge, J. S. (1995). The Geometry and Dynamics of Low-Relief Bed Forms in
581 Heterogeneous Sediment in a Laboratory Channel, and their Relationship to Water Flow and
582 Sediment Transport. *SEPM Journal of Sedimentary Research*, Vol. 65A.
583 <https://doi.org/10.1306/D4268013-2B26-11D7-8648000102C1865D>

584 Best, H., McNamara, J. P., & Liberty, L. (2005). Association of Ice and River Channel Morphology
585 Determined Using Ground-penetrating Radar in the Kuparuk River, Alaska. *Arctic, Antarctic, and*
586 *Alpine Research*, 37(2), 157–162. [https://doi.org/10.1657/1523-](https://doi.org/10.1657/1523-0430(2005)037[0157:AOIARC]2.0.CO;2)
587 [0430\(2005\)037\[0157:AOIARC\]2.0.CO;2](https://doi.org/10.1657/1523-0430(2005)037[0157:AOIARC]2.0.CO;2)

588 Bridge, J. S. (1993). The interaction between channel geometry, water flow, sediment transport and
589 deposition in braided rivers. *Geological Society, London, Special Publications*, 75(1), 13–71.
590 <https://doi.org/10.1144/GSL.SP.1993.075.01.02>

591 Brinkerhoff, C. B., Gleason, C. J., & Ostendorf, D. W. (2019). Reconciling at-a-Station and at-Many-
592 Stations Hydraulic Geometry Through River-Wide Geomorphology. *Geophysical Research Letters*,
593 46(16), 9637–9647. <https://doi.org/10.1029/2019GL084529>

594 Daly, C., Helmer, E. H., & Quiñones, M. (2003). Mapping the climate of Puerto Rico, Vieques and Culebra:
595 CLIMATE MAPPING. *International Journal of Climatology*, 23(11), 1359–1381.
596 <https://doi.org/10.1002/joc.937>

597 David, G. C. L., Wohl, E., Yochum, S. E., & Bledsoe, B. P. (2010). Controls on at-a-station hydraulic
598 geometry in steep headwater streams, Colorado, USA. *Earth Surface Processes and Landforms*,
599 35(15), 1820–1837. <https://doi.org/10.1002/esp.2023>

600 Dingman, S. L. (2007). Analytical derivation of at-a-station hydraulic–geometry relations. *Journal of*
601 *Hydrology*, 334(1–2), 17–27. <https://doi.org/10.1016/j.jhydrol.2006.09.021>

602 Dingman, S. L., & Afshari, S. (2018). Field verification of analytical at-a-station hydraulic-geometry
603 relations. *Journal of Hydrology*, 564, 859–872. <https://doi.org/10.1016/j.jhydrol.2018.07.020>

604 Doll, B. A., Wise-Frederick, D. E., Buckner, C. M., Wilkerson, S. D., Harman, W. A., Smith, R. E., &
605 Spooner, J. (2002). HYDRAULIC GEOMETRY RELATIONSHIPS FOR URBAN STREAMS
606 THROUGHOUT THE PIEDMONT OF NORTH CAROLINA. *Journal of the American Water*
607 *Resources Association*, 38(3), 641–651. <https://doi.org/10.1111/j.1752-1688.2002.tb00986.x>

608

609 Falcone, J.A., 2011, GAGES-II: Geospatial Attributes of Gages for Evaluating Streamflow. Digital spatial
610 data set, http://water.usgs.gov/GIS/metadata/usgswrd/XML/gagesII_Sept2011.xml.

611 Ferguson, R. I. (1986). Hydraulics and hydraulic geometry. *Progress in Physical Geography: Earth and*
612 *Environment*, 10(1), 1–31. <https://doi.org/10.1177/030913338601000101>

613 Fitzpatrick, F. A., & Knox, J. C. (2000). SPATIAL AND TEMPORAL SENSITIVITY OF
614 HYDROGEOMORPHIC RESPONSE AND RECOVERY TO DEFORESTATION,
615 AGRICULTURE, AND FLOODS. *Physical Geography*, 21(2), 89–108.
616 <https://doi.org/10.1080/02723646.2000.10642701>

617 Gleason, C. J. (2015). Hydraulic geometry of natural rivers: A review and future directions. *Progress in*
618 *Physical Geography: Earth and Environment*, 39(3), 337–360.
619 <https://doi.org/10.1177/0309133314567584>

620 Gleason, C. J., & Smith, L. C. (2014). Toward global mapping of river discharge using satellite images and
621 at-many-stations hydraulic geometry. *Proceedings of the National Academy of Sciences*, 111(13),
622 4788–4791. <https://doi.org/10.1073/pnas.1317606111>

623 Guan, M., Carrivick, J. L., Wright, N. G., Sleigh, P. A., & Staines, K. E. H. (2016). Quantifying the
624 combined effects of multiple extreme floods on river channel geometry and on flood hazards.
625 *Journal of Hydrology*, 538, 256–268. <https://doi.org/10.1016/j.jhydrol.2016.04.004>

626 Huang, Q., Long, D., Du, M., Zeng, C., Qiao, G., Li, X., Hou, A., & Hong, Y. (2018). Discharge estimation
627 in high-mountain regions with improved methods using multisource remote sensing: A case study
628 of the Upper Brahmaputra River. *Remote Sensing of Environment*, 219, 115–134.
629 <https://doi.org/10.1016/j.rse.2018.10.008>

630 Jia, Y., Yi, Y., Li, Z., Wang, Z., & Zheng, X. (2017). Integrating hydraulic equivalent sections into a
631 hydraulic geometry study. *Journal of Hydrology*, 552, 407–420.
632 <https://doi.org/10.1016/j.jhydrol.2017.06.039>

633 Jowett, I. G. (1998). Hydraulic geometry of New Zealand rivers and its use as a preliminary method of
634 habitat assessment. *Regulated Rivers: Research & Management: An International Journal Devoted*
635 *to River Research and Management*, 14.5, 451–466. [https://doi.org/10.1002/\(SICI\)1099-](https://doi.org/10.1002/(SICI)1099-1646(199809)14:5<451::AID-RRR512>3.0.CO;2-1)
636 [1646\(199809\)14:5<451::AID-RRR512>3.0.CO;2-1](https://doi.org/10.1002/(SICI)1099-1646(199809)14:5<451::AID-RRR512>3.0.CO;2-1)

637 Kale, V. S., & Hire, P. S. (2004). Effectiveness of monsoon floods on the Tapi River, India: Role of channel
638 geometry and hydrologic regime. *Geomorphology*, 57(3–4), 275–291.
639 [https://doi.org/10.1016/S0169-555X\(03\)00107-7](https://doi.org/10.1016/S0169-555X(03)00107-7)

640 Kendall, M. G. (1938). A New Measure of Rank Correlation. *Biometrika*, 30(1/2), 81.
641 <https://doi.org/10.2307/2332226>

642 Klein, M. (1981). Drainage area and the variation of channel geometry downstream. *Earth Surface*
643 *Processes and Landforms*, 6(6), 589–593. <https://doi.org/10.1002/esp.3290060608>

644 Knighton, D., & Wharton. (2014). *Fluvial Forms and Processes: A New Perspective* (2nd ed.). Routledge.
645 <https://doi.org/10.4324/9780203784662>

646 Landsea, C. W., & Franklin, J. L. (2013). Atlantic Hurricane Database Uncertainty and Presentation of a
647 New Database Format. *Monthly Weather Review*, 141(10), 3576–3592.
648 <https://doi.org/10.1175/MWR-D-12-00254.1>

649 Lee, L., Lees, M., & Ridenour, G. S. (2019). Multi-Interval Data Mining of At-A-Station Hydraulic
650 Geometry to Quantify Temporal Stability. *2019 IEEE 10th Annual Information Technology,
651 Electronics and Mobile Communication Conference (IEMCON)*, 0501–0508.
652 <https://doi.org/10.1109/IEMCON.2019.8936151>

653 Leopold, L. B., & Maddock, T. (1953). *The hydraulic geometry of stream channels and some physiographic
654 implications* (Vol. 252). US Government Printing Office.

655 Leopold, L. B., & Miller, J. P. (1956). *Ephemeral streams—Hydraulic factors and their relation to the
656 drainage net* (Vol. 282). US Government Printing Office.

657 Leopold, L. B., Wolman, M. G., & Miller, J. P. (1964). *Fluvial processes in geomorphology*. Freeman.

658 Lewis, L. A. (1969). SOME FLUVIAL GEOMORPHIC CHARACTERISTICS OF THE MANATI BASIN,
659 PUERTO RICO. *Annals of the Association of American Geographers*, 59(2), 280–293.
660 <https://doi.org/10.1111/j.1467-8306.1969.tb00671.x>

661 Li, Y., Wright, D. B., & Byrne, P. K. (2020). The Influence of Tropical Cyclones on the Evolution of River
662 Conveyance Capacity in Puerto Rico. *Water Resources Research*, 56(9).
663 <https://doi.org/10.1029/2020WR027971>

664 Malkinson, D., & Wittenberg, L. (2007). Scaling the effects of riparian vegetation on cross-sectional
665 characteristics of ephemeral mountain streams—A case study of Nahal Oren, Mt. Carmel, Israel.
666 *CATENA*, 69(2), 103–110. <https://doi.org/10.1016/j.catena.2006.04.026>

667 Millar, R. G., & Quick, M. C. (1993). Effect of Bank Stability on Geometry of Gravel Rivers. *Journal of
668 Hydraulic Engineering*, 119(12), 1343–1363. [https://doi.org/10.1061/\(ASCE\)0733-
669 9429\(1993\)119:12\(1343\)](https://doi.org/10.1061/(ASCE)0733-9429(1993)119:12(1343))

670 Montgomery, D. R., & Buffington, J. M. (1997). Channel-reach morphology in mountain drainage basins.
671 *Geological Society of America Bulletin*, 16.

672 Montgomery, D. R., & MacDonald, L. H. (2002). DIAGNOSTIC APPROACH TO STREAM CHANNEL
673 ASSESSMENT AND MONITORING. *Journal of the American Water Resources Association*,
674 38(1), 1–16. <https://doi.org/10.1111/j.1752-1688.2002.tb01530.x>

675 Morel, M., Booker, D. J., Gob, F., & Lamouroux, N. (2020a). Intercontinental predictions of river hydraulic
676 geometry from catchment physical characteristics. *Journal of Hydrology*, 582, 124292.
677 <https://doi.org/10.1016/j.jhydrol.2019.124292>

678 Morel, M., Booker, D. J., Gob, F., & Lamouroux, N. (2020b). Consistent Theoretical and Empirical
679 Predictions of at-a-Station Hydraulic Geometry Exponents in Stream Reaches. *Water Resources*
680 *Research*, 56(10). <https://doi.org/10.1029/2020WR027242>

681 Morel, M., Tamisier, V., Pella, H., Booker, D. J., Navratil, O., Piégay, H., Gob, F., & Lamouroux, N. (2019).
682 Revisiting the drivers of at-a-station hydraulic geometry in stream reaches. *Geomorphology*, 328,
683 44–56. <https://doi.org/10.1016/j.geomorph.2018.12.007>

684 National Oceanic and Atmospheric Administration. (2021). *National Weather Service*.

685 OCM Partners. (2019). 2016–2017 USGS Lidar DEM: Puerto Rico. *Charleston, SC: NOAA National*
686 *Centers for Environmental Information*. <https://www.fisheries.noaa.gov/inport/item/55314>

687 Ogden, F. L. (2016). Evidence of equilibrium peak runoff rates in steep tropical terrain on the island of
688 Dominica during Tropical Storm Erika, August 27, 2015. *Journal of Hydrology*, 542, 35–46.
689 <https://doi.org/10.1016/j.jhydrol.2016.08.041>

690 Park, C. C. (1977). World-wide variations in hydraulic geometry exponents of stream channels: An analysis
691 and some observations. *Journal of Hydrology*, 33(1–2), 133–146. [https://doi.org/10.1016/0022-](https://doi.org/10.1016/0022-1694(77)90103-2)
692 [1694\(77\)90103-2](https://doi.org/10.1016/0022-1694(77)90103-2)

693 Phillips, C. B., & Scatena, F. N. (2013). Reduced channel morphological response to urbanization in a
694 flood-dominated humid tropical environment: REDUCED CHANNEL MORPHOLOGICAL
695 RESPONSE TO URBANIZATION. *Earth Surface Processes and Landforms*, 38(9), 970–982.
696 <https://doi.org/10.1002/esp.3345>

697 Qin, C., Wu, B., Wang, Y., Fu, X., Xue, Y., Li, D., Li, M., & Zhang, Y. (2020). Dynamic variability of at-
698 a-station hydraulic-geometry for mountain rivers in the southeast Qinghai-Tibet Plateau: The cases
699 of Yalong River and upper Jinsha River. *CATENA*, 194, 104723.
700 <https://doi.org/10.1016/j.catena.2020.104723>

701 R core team. (2020). *R: A language and environment for statistical computing*. (4.0.3) [Computer software].
702 R Foundation for Statistical Computing. <https://www.R-project.org/>

703 Ran, L., Wang, S., & Lu, X. X. (2012). Hydraulic geometry change of a large river: A case study of the
704 upper Yellow River. *Environmental Earth Sciences*, 66(4), 1247–1257.
705 <https://doi.org/10.1007/s12665-011-1336-x>

706 Reid, D. E., Hickin, E. J., & Babakaiff, S. C. (2010). Low-flow hydraulic geometry of small, steep mountain
707 streams in southwest British Columbia. *Geomorphology*, 122(1–2), 39–55.
708 <https://doi.org/10.1016/j.geomorph.2010.05.012>

709 Reisenbüchler, M., Bui, M. D., Skublics, D., & Rutschmann, P. (2019). An integrated approach for
710 investigating the correlation between floods and river morphology: A case study of the Saalach
711 River, Germany. *Science of The Total Environment*, 647, 814–826.
712 <https://doi.org/10.1016/j.scitotenv.2018.08.018>

713 Shen, C., Wang, S., & Liu, X. (2016). Geomorphological significance of at-many-stations hydraulic
714 geometry: Physical Interpretations of AMHG. *Geophysical Research Letters*, 43(8), 3762–3770.
715 <https://doi.org/10.1002/2016GL068364>

716 Slater, L. J., Singer, M. B., & Kirchner, J. W. (2015). Hydrologic versus geomorphic drivers of trends in
717 flood hazard. *Geophysical Research Letters*, 42(2), 370–376.
718 <https://doi.org/10.1002/2014GL062482>

719 Smith, J. A., Sturdevant-Rees, P., Baeck, M. L., & Larsen, M. C. (2005). Tropical cyclones and the flood
720 hydrology of Puerto Rico: TROPICAL CYCLONES AND FLOOD HYDROLOGY OF PUERTO
721 RICO. *Water Resources Research*, 41(6). <https://doi.org/10.1029/2004WR003530>

722 Stewardson, M. (2005). Hydraulic geometry of stream reaches. *Journal of Hydrology*, 306(1–4), 97–111.
723 <https://doi.org/10.1016/j.jhydrol.2004.09.004>

724 Su, T., Wang, S., Mei, Y., & Shao, W. (2015). Comparison of channel geometry changes in Inner
725 Mongolian reach of the Yellow River before and after joint operation of large upstream reservoirs.
726 *Journal of Geographical Sciences*, 25(8), 930–942. <https://doi.org/10.1007/s11442-015-1211-x>

727 Turowski, J. M., Hovius, N., Wilson, A., & Horng, M.-J. (2008). Hydraulic geometry, river sediment and
728 the definition of bedrock channels. *Geomorphology*, 99(1–4), 26–38.
729 <https://doi.org/10.1016/j.geomorph.2007.10.001>

730 U.S. Geological Survey. (2006). *National Hydrography Dataset (version 01_05)*.
731 https://nhdplus.com/NHDPlus/NHDPlusV1_21.php

732 U.S. Geological Survey. (2021a). *Peak Streamflow for the Nation*.
733 <https://nwis.waterdata.usgs.gov/usa/nwis/peak>

734 U.S. Geological Survey. (2021b). *Streamflow Measurements for the Nation*.
735 <https://waterdata.usgs.gov/nwis/measurements>

736 Wang, L., Sichangi, A. W., Zeng, T., Li, X., Hu, Z., & Genanu, M. (2019). New methods designed to
737 estimate the daily discharges of rivers in the Tibetan Plateau. *Science Bulletin*, 64(7), 418–421.
738 <https://doi.org/10.1016/j.scib.2019.03.015>

739 Wang, S., Hassan, M. A., & Xie, X. (2006). Relationship between suspended sediment load, channel
740 geometry and land area increment in the Yellow River Delta. *CATENA*, 65(3), 302–314.
741 <https://doi.org/10.1016/j.catena.2006.01.003>

742 West, A. J., Lin, C.-W., Lin, T.-C., Hilton, R. G., Liu, S.-H., Chang, C.-T., Lin, K.-C., Galy, A., Sparkes,
743 R. B., & Hovius, N. (2011). Mobilization and transport of coarse woody debris to the oceans
744 triggered by an extreme tropical storm. *Limnology and Oceanography*, 56(1), 77–85.
745 <https://doi.org/10.4319/lo.2011.56.1.0077>

746 Wiman, J., & Almstedt, A. E. (1997). Hydrodynamics, erosion and heat transfer in a pressurized fluidized
747 bed: Influence of pressure, fluidization velocity, particle size and tube bank geometry. *Chemical*
748 *Engineering Science*, 52(16), 2677–2695. [https://doi.org/10.1016/S0009-2509\(97\)00096-1](https://doi.org/10.1016/S0009-2509(97)00096-1)

749 Yousefi, S., Mirzaee, S., Keesstra, S., Surian, N., Pourghasemi, H. R., Zakizadeh, H. R., & Tabibian, S.
750 (2018). Effects of an extreme flood on river morphology (case study: Karoon River, Iran).
751 *Geomorphology*, 304, 30–39. <https://doi.org/10.1016/j.geomorph.2017.12.034>

752 Zhang, W., Wang, W., Zheng, J., Wang, H., Wang, G., & Zhang, J. (2015). Reconstruction of stage–
753 discharge relationships and analysis of hydraulic geometry variations: The case study of the Pearl
754 River Delta, China. *Global and Planetary Change*, 125, 60–70.
755 <https://doi.org/10.1016/j.gloplacha.2014.12.004>